

Targeting Solutions in Bayesian Multi-Objective Optimization: Sequential and Parallel Versions

David Gaudrie^{1,2}, Rodolphe le Riche^{2,3}, Victor Picheny⁴, Benoît Enaux¹, and Vincent Herbert¹

¹Groupe PSA

²École Nationale Supérieure des Mines de Saint-Étienne

³CNRS LIMOS

⁴INRA Toulouse

Abstract

Multi-objective optimization aims at finding trade-off solutions to conflicting objectives. These constitute the Pareto optimal set. In the context of expensive-to-evaluate functions, it is impossible and often non-informative to look for the entire set. As an end-user would typically prefer a certain part of the objective space, we modify the Bayesian multi-objective optimization algorithm which uses Gaussian Processes to maximize the Expected Hypervolume Improvement, to focus the search in the preferred region. The cumulated effects of the Gaussian Processes and the targeting strategy lead to a particularly efficient convergence to the desired part of the Pareto set. To take advantage of parallel computing, a multi-point extension of the targeting criterion is proposed and analyzed.

Keywords: Gaussian Processes, Parsimonious Optimization, Computer Experiments, Preference-Based Optimization, Parallel Optimization

1 Introduction

Multi-objective optimization aims at minimizing m objectives simultaneously: $\min_{\mathbf{x} \in X \subset \mathbb{R}^d} (f_1(\mathbf{x}), \dots, f_m(\mathbf{x}))$.

As these objectives are generally competing, optimal trade-off solutions known as the Pareto optimal set \mathcal{P}_X are sought. These solutions are *non-dominated*: it is not possible to improve one objective without worsening another ($\forall \mathbf{x}^* \in \mathcal{P}_X, \nexists \mathbf{z} \preceq \mathbf{x}^*$). The image of \mathcal{P}_X in the objective space is called the Pareto front, $\mathcal{P}_Y = \{\mathbf{f}(\mathbf{x}), \mathbf{x} \in \mathcal{P}_X\}$. The Ideal and the Nadir points bound the Pareto front and are defined respectively as $\mathbf{I} = (\min_{\mathbf{y} \in \mathcal{P}_Y} y_1, \dots, \min_{\mathbf{y} \in \mathcal{P}_Y} y_m)$ and $\mathbf{N} = (\max_{\mathbf{y} \in \mathcal{P}_Y} y_1, \dots, \max_{\mathbf{y} \in \mathcal{P}_Y} y_m)$.

More theory and concepts in multi-objective optimization can be found in [34, 29].

Multi-objective optimization algorithms aim at constructing the best approximation to \mathcal{P}_Y , called the *empirical* Pareto front (or approximation front) $\widehat{\mathcal{P}}_Y$ which is made of non-dominated observations. At the end of the search, $\widehat{\mathcal{P}}_Y$ is delivered to a Decision Maker (DM) who will choose a solution.

However, when dealing with expensive computer codes, only a few designs \mathbf{x} can be evaluated. In Bayesian optimization, a surrogate for each objective, $Y_j(\cdot)$, is first fitted to an initial Design of Experiments (DoE) evaluated at n locations, $\mathcal{D}_j^n := \{(\mathbf{x}^{(1)}, f_j(\mathbf{x}^{(1)})), \dots, (\mathbf{x}^{(n)}, f_j(\mathbf{x}^{(n)}))\}$, using Gaussian Processes (GP) [24]. Classically, to contain the computational complexity, the metamodels $Y_j(\cdot)$ are assumed to be independent. In [36] dependent GPs have been considered without noticing significant benefits. Information given by $\mathbf{Y}(\cdot) := (Y_1(\cdot), \dots, Y_m(\cdot))^\top$ is used in order to sequentially evaluate new promising inputs with the aim of reaching the Pareto front [26, 25, 13, 32, 37, 31].

As the Pareto set takes up a large part of the design space when many objectives are considered, it may be impossible to compute an accurate approximation to it within the restricted computational budget. It may anyway be irrelevant to provide the whole Pareto set because it will contain many uninteresting solutions from the DM's point of view.

In the current article, we assume that an aspiration point [39] is known. This aspiration point can be implicitly defined as the center of the Pareto front [17] or a neutral point [40] or an extension of it [43, 11]. Alternatively, it can be given by the DM.

The contributions of this work are twofolds. First, we tailor a classical infill criterion used in Bayesian optimization to intensify the search towards the aspiration point. The new criterion is called mEI. Second, we propose and study a multi-point extension to this targeting criterion, named q-mEI. We also explain why a tempting alternative criterion to q-mEI is inappropriate for optimization. These two contributions make the two main parts of the article. Each part contains comparative numerical experiments, illustrating in particular the targeting ability of mEI and the computational gain of q-mEI over mEI.

2 Bayesian multi-objective optimization with sequential targeting

2.1 mEI: a new infill criterion for targeting parts of the objective space

Articulating preferences has already been addressed in multi-objective optimization, see for instance [39, 16, 38, 7, 5]. In Bayesian multi-objective optimization, fitted to costly objectives, new points are sequentially added by maximizing an infill criterion whose purpose is to guide the search towards the Pareto set. At each iteration t , a new point $\mathbf{x}^{(t+1)}$ is selected and evaluated. $\mathbf{x}^{(t+1)}$ and $\mathbf{f}(\mathbf{x}^{(t+1)})$ are used to update the metamodels $Y_j(\cdot)$. The Expected Hypervolume Improvement (EHI, [13]) is a commonly employed multi-objective infill criterion. It chooses the input which maximizes the expected growth of the hypervolume dominated by $\widehat{\mathcal{P}}_{\mathbf{y}}$ up to a reference point \mathbf{R} : $\mathbf{x}^{(t+1)} = \arg \max_{\mathbf{x} \in X} \text{EHI}(\mathbf{x}; \mathbf{R})$, with

$$\text{EHI}(\mathbf{x}; \mathbf{R}) = \mathbb{E}[H(\widehat{\mathcal{P}}_{\mathbf{y}} \cup \{\mathbf{Y}(\mathbf{x})\}; \mathbf{R}) - H(\widehat{\mathcal{P}}_{\mathbf{y}}; \mathbf{R})]$$

where

$$H(\mathcal{A}; \mathbf{R}) = \text{Vol}\left(\bigcup_{\mathbf{y} \in \mathcal{A}} \{\mathbf{z} : \mathbf{y} \preceq \mathbf{z} \preceq \mathbf{R}\}\right)$$

is the hypervolume indicator of the set \mathcal{A} up to \mathbf{R} [44]. Classically, \mathbf{R} is taken beyond the observed Nadir, e.g. [32], in order to cover the entire front. As shown in Figure 1 and already investigated in [3, 21, 4, 14], the choice of \mathbf{R} has a huge impact: the farthest from the (empirical) Pareto front, the more the edges are emphasized.

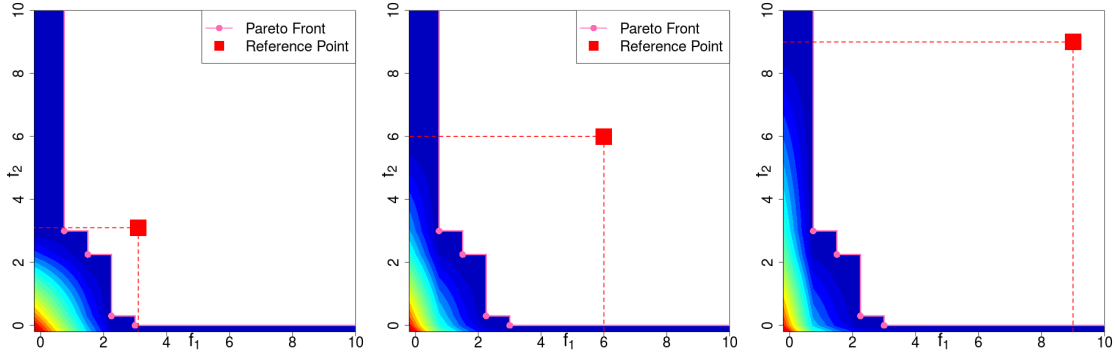


Figure 1: Hypervolume Improvement in a bi-objective case for three different reference points. Moving \mathbf{R} (red square) away from the Pareto front gives a higher relative importance to the edges of the Pareto front.

Previous works in Bayesian multi-objective optimization have also targeted particular areas of the objective space thanks to ad-hoc infill criteria. The Weighted expected Hypervolume Improvement (WHI) [9, 1, 2, 10] is a variant of EHI that emphasizes given parts of the objective space through a user-defined weighting function. In [42, 41], a Truncated EHI criterion, which restricts the Gaussian distribution to a user-supplied hyperbox in which new solutions are sought, is studied.

Our approach targets specific parts of the Pareto front with EHI by solely controlling the reference point \mathbf{R} . Indeed, the choice of \mathbf{R} is instrumental in deciding the combination of objectives for which *improvement* occurs: $\mathcal{I}_{\mathbf{R}} := \{\mathbf{y} \in \mathbb{R}^m : \mathbf{y} \preceq \mathbf{R}\}$. EHI's search favors objective vectors that dominate \mathbf{R} , that we set at the provided or implicitly determined aspiration point.

When the objectives are modeled by independent GPs and the employed reference point is not dominated by the empirical front, $\widehat{\mathcal{P}}_{\mathbf{y}} \not\prec \mathbf{R}$ (in the sense that no vector in $\widehat{\mathcal{P}}_{\mathbf{y}}$ dominates \mathbf{R}), one has $\text{EHI}(\cdot; \mathbf{R}) = \text{mEI}(\cdot; \mathbf{R})$, where mEI stands for the product of the famous mono-objective Expected Improvement (EI) [24] considering \mathbf{R} as the observed minimum in each objective,

$$\text{mEI}(\mathbf{x}; \mathbf{R}) := \prod_{j=1}^m \text{EI}_j(\mathbf{x}; R_j). \quad (1)$$

The proof is straightforward and given in [17]. This observation is particularly appealing from a computational point of view: EHI requires the computation of m -dimensional hypervolumes involving expensive Monte-Carlo estimations in a many-objective case. On the contrary, an analytical expression for mEI and even its gradient are available to efficiently maximize it.

Figure 2 compares the Improvement functions, whose expected values correspond to EHI and to mEI, in a two-dimensional objective space. EHI naturally takes the Pareto front into account, contrarily to mEI, for which \mathbf{R} has to be set up accordingly to the user's preferences. Both criteria are equivalent when \mathbf{R} is non-dominated.

Using a non-dominated reference point in the spirit of an aspiration level, EHI is replaced by mEI. At each iteration t , $\mathbf{x}^{(t+1)} = \arg \max_{\mathbf{x} \in X} \text{mEI}(\mathbf{x}; \mathbf{R})$, the most promising design to improve upon \mathbf{R} , is computed and evaluated by the expensive functions. The metamodels are updated using this additional information. In order to stay non-dominated, \mathbf{R} must potentially be updated.

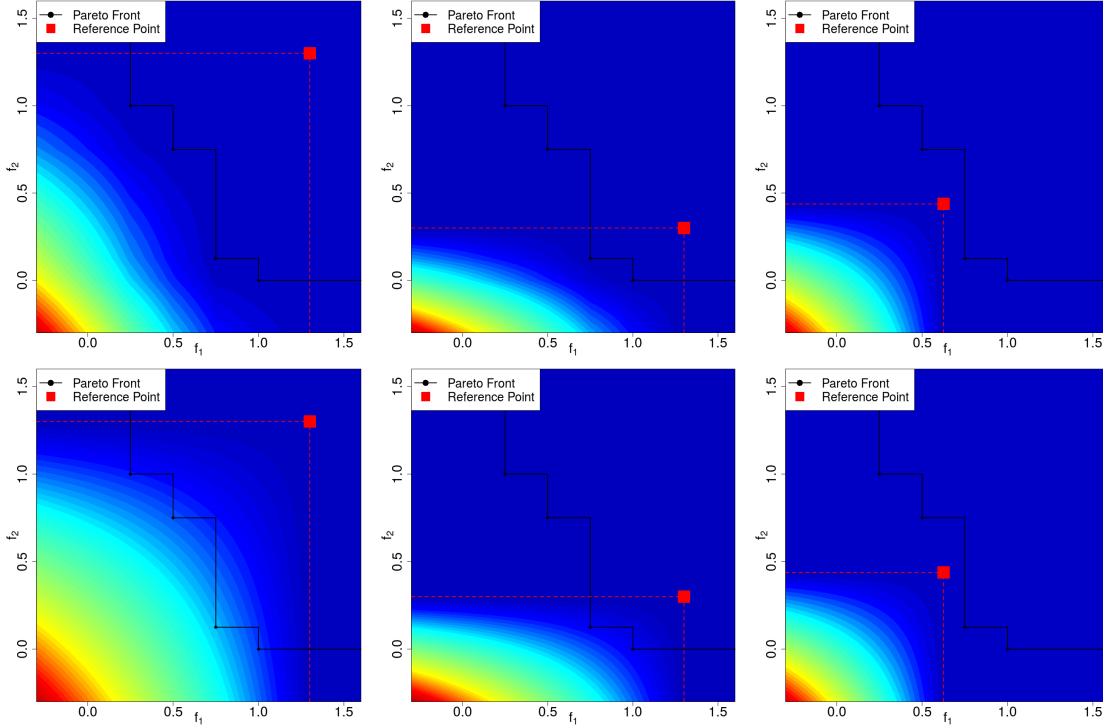


Figure 2: Comparison of the Improvement functions in the objective space \mathbb{R}^2 . EHI is the expected value of the Hypervolume Improvement (top) and mEI is the expected value of the product of improvements over \mathbf{R} (bottom). On the left, the reference point (red square) is dominated by the whole front. The Hypervolume Improvement takes the empirical Pareto front (black) into account contrarily to the product of Improvements over \mathbf{R} . In the middle, \mathbf{R} is only dominated by two points. As the Improvement functions equal zero when $f_2 > 0.3$, using this \mathbf{R} will promote solutions with small f_2 values. On the right, the reference point is non-dominated and the two improvement functions are the same.

Targeting a particular part of the Pareto front leads to a fast local convergence. Once \mathbf{R} is on the real Pareto front, the algorithm will try to improve non-improvable values (see left of Figure 4). To avoid wasting costly evaluations, the convergence has to be checked. To this aim, we estimate $p(\mathbf{y})$, the probability of dominating the objective vector \mathbf{y} , simulating Pareto fronts through conditional GPs. Like the Vorob'ev deviation [30] used in [6], $p(\mathbf{y})(1 - p(\mathbf{y}))$ is a measure of domination uncertainty, which tends to 0 as $p(\mathbf{y})$ tends to 0 or 1. We assume local convergence when the *line-uncertainty*, $\int_{\mathcal{L}} p(\mathbf{y})(1 - p(\mathbf{y}))d\mathbf{y}$, is small enough, where \mathcal{L} is a line going through \mathbf{I} and \mathbf{R} , and crossing the empirical front. The convergence detection is described more thoroughly in [17]. In practice, it is used as a convergence criterion to stop the algorithm.

Although any non-dominated \mathbf{R} defines a valid acquisition function $\text{mEI}(\cdot; \mathbf{R})$, our implementation (see Algorithm 1) uses the center of the front (described in the next Section), $\mathbf{R} \equiv \widehat{\mathbf{C}}$, and is called C-EHI. In this case, \mathcal{L} is the line from the Ideal to the Nadir point.

2.2 Well-balanced solutions: the center of the Pareto front

If the preferences of the DM are not explicitly known through a reference point and the associated targeted region $\mathcal{I}_{\mathbf{R}}$, we argue that “well-balanced” solutions are the most interesting ones. In the same vein as [8] where the authors implicitly prefer knee points, we direct the search towards well-balanced solutions in the absence of preferences. Well-balanced solutions belong to the central part of the Pareto front, defined in the following paragraph, and have equilibrated trade-offs between the objectives.

Definition. We define the center, \mathbf{C} , of the Pareto front as the projection (intersection in case of a continuous front) of the closest non-dominated point on the Ideal-Nadir line (in the Euclidean objective space). An example of Pareto front center can be seen in Figure 3. This center corresponds visually to an equilibrium among all objectives. Alternative definitions involving e.g. the barycenter of the Pareto front, are likely to be harder to calculate in high-dimensional spaces. Furthermore, this center has the property of being insensitive to a linear scaling of the objectives in a bi-objective case¹. \mathbf{C} is also very little sensitive to perturbations of the Ideal or the Nadir point: under mild regularity conditions on the Pareto front, $|\frac{\partial C_i}{\partial I_j}|$ and $|\frac{\partial C_i}{\partial N_j}| < 1$, $i, j = 1, \dots, m$.

Estimation. As the Ideal and the Nadir of the empirical Pareto front will sometimes be weak substitutes for the real ones (leading to a biased estimated center), those two points have to be truly estimated for the purpose of computing the center. The probabilistic nature of the metamodels (GPs) allows to simulate possible responses of the objective functions. Conditional GP simulations are thus performed to create possible Pareto fronts, each of which defines a sample for \mathbf{I} and \mathbf{N} . The estimated Ideal and Nadir are the medians of the samples. The intersection between the line $\hat{\mathcal{L}}$ joining those points and the empirical Pareto front (or the projection if there is no intersection) is the estimated center $\hat{\mathbf{C}}$.

More properties concerning the center of the Pareto front, and more details regarding its computation via \mathbf{I} and \mathbf{N} 's estimation are given in [17].

2.3 Experiment: targeting the center of the Pareto front with mEI

We apply the proposed methodology with $\mathbf{R} = \hat{\mathbf{C}}$ to a benchmark built from real-world airfoil aerodynamic data described in [17], the Meta NACA. The chosen version of the problem has $d = 8$ dimensions and $m = 2$ objectives, the negative lift and the drag, to be minimized. Figure 4 shows that, compared with standard techniques, the proposed methodology leads to a faster and a more precise convergence to the central part of the Pareto front at the cost of a narrower covering of the front. The results are shown at the iteration which triggers the convergence criterion: only marginal gains would indeed be obtained by continuing to target the same region. Figure 3 indicates how \mathbf{R} evolves to direct the search to the true center of the Pareto front, \mathbf{C} .

¹ Non-sensitivity to a linear scaling of the objectives is true when the Pareto front intersects the Ideal-Nadir line. Without intersection, exceptions may occur for $m \geq 3$.

Center-Targeting Algorithm (C-EHI)
 Create and evaluate an initial DoE of n designs;
 Initialize m GPs $Y_j(\cdot)$ for each objective
 $f_j(\cdot), j = 1, \dots, m$;
 $t = 1$; $line-uncertainty = +\infty$;
while ($line-uncertainty > \varepsilon$) **and** ($t \leq budget$) **do**
 estimate \mathbf{I} , \mathbf{N} and \mathbf{C} ;
 $\mathbf{x}^{(n+t)} = \arg \max_{\mathbf{x} \in X} mEI(\mathbf{x}; \mathbf{C})$;
 evaluate $f_j(\mathbf{x}^{(n+t)})$ and update the GPs;
 compute $line-uncertainty(\mathbf{Y}(\cdot), \mathbf{I}, \mathbf{N})$;
 $t = t + 1$;
end

Algorithm 1: Targeting Algorithm

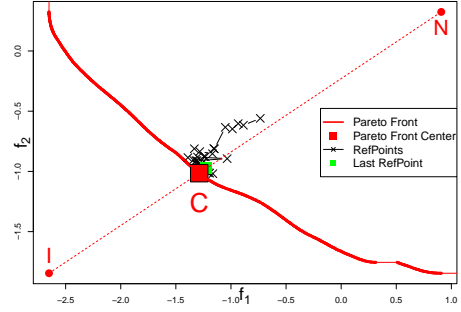


Figure 3: Reference points \mathbf{R} successively used for directing the search during one C-EHI run. They lie close to the dashed Ideal-Nadir line (\mathbf{IN}) and lead the algorithm to the center of the Pareto front (\mathbf{C}).

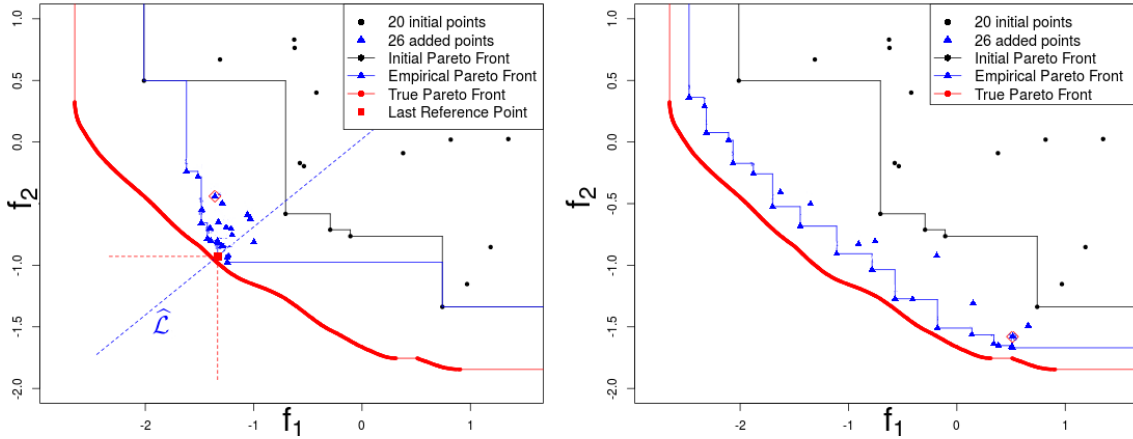


Figure 4: Bi-objective optimization with C-EHI (left). The initial approximation (black) has mainly been improved around the center. Compared with a standard EHI (right), the proposed methodology achieves convergence to the central part of the front. EHI considers more compromises between objectives, but cannot converge within the given budget (26 evaluations).

3 Bayesian multi-objective optimization with parallel targeting

In the context of costly objective functions, it seems likely that the temporal efficiency of Bayesian optimization algorithms can be improved by evaluating the functions in parallel (on different computers or on a cluster) whenever possible. A parallel version of these algorithms directly stems from replacing the infill criteria with their multi-point pendants: if q points are produced by the

maximization of the infill criterion, the $\mathbf{f}(\cdot)$'s can then be calculated in parallel. In some cases, there is a side benefit to the multi-point criterion in that it makes the algorithms more robust to inadequacies between the GPs and the true functions by spreading the points at each iteration while still complying with the infill criteria logic. An example of multi-point criterion in sequential computing can be found in Chapter 3 of [33].

The multi-point Expected Improvement (q-EI) introduced in [35] searches an optimal batch of q points, instead of looking for solely one. In [20] it is defined as

$$\text{q-EI}(\{\mathbf{x}^{(t+1)}, \dots, \mathbf{x}^{(t+q)}\}) = \mathbb{E}[\max_{i=1, \dots, q} (f_{\min} - Y(\mathbf{x}^{(t+i)}))_+] = \mathbb{E}[(f_{\min} - \min_{i=1, \dots, q} Y(\mathbf{x}^{(t+i)}))_+] \quad (2)$$

$\{\mathbf{x}^{(t+1)*}, \dots, \mathbf{x}^{(t+q)*}\}$ maximizing (2) are q promising points to evaluate simultaneously. It is clear from the q-EI criterion that the price to pay for multi-point infill criteria is an increase in the dimension of the inner optimization loop that creates the next iterates. In Algorithm 1, the next iterate $\mathbf{x}^{(t+1)}$ results from an optimization in d dimensions, while in a q -points algorithm there are $d \times q$ dimensions.

The multi-point Expected Improvement has received some attention recently, see for instance [19, 18, 22, 23, 15], where the criterion is computed using Monte-Carlo simulations. It has been calculated in closed form for $q = 2$ in [20] and extended for any q in [12]. An expression and a proxy for its gradient [27, 28] have then been calculated for efficiently maximizing it in X^q .

In the same spirit, we wish to extend the mEI criterion so that it returns q designs to evaluate in parallel.

3.1 The mq-EI criterion: a naive extension

The mEI being a product of EI's, a first approach to extend the mEI criterion to a batch of q points is to use the product of single-objective q-EI's (called mq-EI for "multiplicative q-EI") using R_j instead of $\min_{i=1, \dots, t} f_j(\mathbf{x}^{(i)})$ in (2):

$$\begin{aligned} \text{mq-EI}(\{\mathbf{x}^{(t+1)}, \dots, \mathbf{x}^{(t+q)}\}; \mathbf{R}) &= \prod_{j=1}^m \text{q-EI}_j(\{\mathbf{x}^{(t+1)}, \dots, \mathbf{x}^{(t+q)}\}; R_j) \\ &= \prod_{j=1}^m \mathbb{E}[\max_{i=1, \dots, q} (R_j - Y_j(\mathbf{x}^{(t+i)}))_+] = \mathbb{E}[\prod_{j=1}^m \max_{i=1, \dots, q} (R_j - Y_j(\mathbf{x}^{(t+i)}))_+] \end{aligned} \quad (3)$$

because the $Y_j(\cdot)$'s are assumed independent. This criterion has however the drawback of not using a product of joint improvement in all objectives, as the max among the q points is taken independently for each objective j considered. This may lead to undesirable behaviors: the batch of q optimal points using this criterion may be composed of optimal points w.r.t. each individual EI_j . For example with $m = 2$ and $q = 2$, a batch $\{\mathbf{x}^{(1)*}, \mathbf{x}^{(2)*}\}$ with promising $Y_1(\mathbf{x}^{(1)*})$ and $Y_2(\mathbf{x}^{(2)*})$ may be optimal, without taking $Y_2(\mathbf{x}^{(1)*})$ and $Y_1(\mathbf{x}^{(2)*})$ into account. $\mathbf{x}^{(1)*}$ and $\mathbf{x}^{(2)*}$ may not even dominate \mathbf{R} while scoring a high mq-EI. For these reasons, the mq-EI criterion breaks the coupling through \mathbf{x} between the functions, allocating marginally each point to an objective. mq-EI does not tackle multi-objective problems.

3.2 The q-mEI criterion

Following the definition of q-EI (2), a proper multi-point extension of mEI (1) is

$$\text{q-mEI}(\{\mathbf{x}^{(t+1)}, \dots, \mathbf{x}^{(t+q)}\}; \mathbf{R}) = \mathbb{E} \left[\max_{i=1, \dots, q} \left(\prod_{j=1}^m (R_j - Y_j(\mathbf{x}^{(t+i)}))_+ \right) \right] \quad (4)$$

3.3 Properties of both criteria

In this part, we study some properties and bounds for both proposed criteria.

Proposition 1. When evaluated twice at the same design, m-qEI and qm-EI reduce to mEI: $\text{mq-EI}(\{\mathbf{x}, \mathbf{x}\}; \mathbf{R}) = \text{q-mEI}(\{\mathbf{x}, \mathbf{x}\}; \mathbf{R}) = \text{mEI}(\mathbf{x}; \mathbf{R})$

Proof:

$$\begin{aligned} \text{mq-EI}(\{\mathbf{x}, \mathbf{x}\}; \mathbf{R}) &= \prod_{j=1}^m \text{q-EI}_j(\{\mathbf{x}, \mathbf{x}\}; R_j) = \prod_{j=1}^m \text{EI}_j(\mathbf{x}; R_j) = \text{mEI}(\mathbf{x}; \mathbf{R}). \\ \text{q-mEI}(\{\mathbf{x}, \mathbf{x}\}; \mathbf{R}) &= \mathbb{E}[\prod_{j=1}^m (R_j - Y_j(\mathbf{x}))_+] = \text{mEI}(\mathbf{x}; \mathbf{R}). \quad \square \end{aligned}$$

Proposition 2. When $\mathcal{P}_y \not\subseteq \mathbf{R}$, q-mEI calculated at two training points \mathbf{x} and \mathbf{x}' is null. q-mEI calculated at one training point \mathbf{x} and one new point \mathbf{x}'' reduces to mEI at the latter: $\text{q-mEI}(\{\mathbf{x}, \mathbf{x}'\}; \mathbf{R}) = 0$, $\text{q-mEI}(\{\mathbf{x}, \mathbf{x}''\}; \mathbf{R}) = \text{mEI}(\mathbf{x}''; \mathbf{R})$

Proof:

As \mathbf{x} and \mathbf{x}' are training points, $\mathbf{Y}(\mathbf{x})$ and $\mathbf{Y}(\mathbf{x}')$ are no longer random variables, and the expectation vanishes. Since \mathbf{R} is not dominated by the observed values $\mathbf{y} = \mathbf{Y}(\mathbf{x})$ and $\mathbf{y}' = \mathbf{Y}(\mathbf{x}')$, $\prod_{j=1}^m (R_j - Y_j(\mathbf{x}))_+ = \prod_{j=1}^m (R_j - y_j)_+ = 0$ and the same occurs with \mathbf{y}' . Finally, $\text{q-mEI}(\{\mathbf{x}, \mathbf{x}'\}; \mathbf{R}) = 0$.

In the case of one observed \mathbf{x} and one unobserved \mathbf{x}'' , $\prod_{j=1}^m (R_j - Y_j(\mathbf{x}''))_+ \geq \prod_{j=1}^m (R_j - Y_j(\mathbf{x}))_+ = 0$, and $\text{q-mEI}(\{\mathbf{x}, \mathbf{x}''\}; \mathbf{R}) = \mathbb{E}[\prod_{j=1}^m (R_j - Y_j(\mathbf{x}''))_+] = \text{mEI}(\mathbf{x}''; \mathbf{R})$. \square

Even though these properties seem obvious and mandatory for a multi-point infill criterion, they do not hold for mq-EI. To see this, let us consider a case with $m = 2$ objectives, \mathbf{R} a non-dominated reference point, and \mathbf{x} and \mathbf{x}' two evaluated designs with responses $\mathbf{y} = \mathbf{f}(\mathbf{x}) = (y_1, y_2)^\top$, $\mathbf{y}' = \mathbf{f}(\mathbf{x}') = (y'_1, y'_2)^\top$, satisfying $y_1 < R_1 < y'_1$ and $y'_2 < R_2 < y_2$. By definition, $\text{mq-EI}(\{\mathbf{x}, \mathbf{x}'\}; \mathbf{R}) = \prod_{j=1}^2 \mathbb{E}[\max((R_j - y_j)_+, (R_j - y'_j)_+)] = (R_1 - y_1)(R_2 - y'_2) > 0$. Furthermore, $\text{mq-EI}(\{\mathbf{x}, \mathbf{x}''\}; \mathbf{R}) = \prod_{j=1}^2 \mathbb{E}[\max((R_j - y_j)_+, (R_j - Y_j(\mathbf{x}''))_+)] = \text{EI}_2(\mathbf{x}''; R_2) \times \mathbb{E}[\max((R_1 - y_1), (R_1 - Y_1(\mathbf{x}''))_+)] > \text{EI}_2(\mathbf{x}''; R_2) \times \text{EI}_1(\mathbf{x}''; R_1) = \text{mEI}(\mathbf{x}''; \mathbf{R})$.

Some bounds can also be computed. We assume $q \geq m$ which will usually be verified. Let us denote $\mathbf{x}^{(j)*}$ the maximizers of $\text{EI}_j(\cdot; R_j)$ for $j = 1, \dots, m$; $\mathbf{x}^{(m+1)*}, \dots, \mathbf{x}^{(q)*}$ any other points and \mathbf{x}^* the maximizer of $\text{mEI}(\cdot; \mathbf{R})$. Then,

$$\begin{aligned} \max_{\mathbf{x}^{(1)}, \dots, \mathbf{x}^{(q)}} \text{mq-EI}(\{\mathbf{x}^{(1)}, \dots, \mathbf{x}^{(q)}\}; \mathbf{R}) &= \max_{\mathbf{x}^{(1)}, \dots, \mathbf{x}^{(q)}} \prod_{j=1}^m \text{q-EI}_j(\{\mathbf{x}^{(1)}, \dots, \mathbf{x}^{(q)}\}; R_j) \\ &\geq \prod_{j=1}^m \text{q-EI}_j(\{\mathbf{x}^{(1)*}, \dots, \mathbf{x}^{(m)*}, \mathbf{x}^{(m+1)*}, \dots, \mathbf{x}^{(q)*}\}; R_j) \geq \prod_{j=1}^m \text{EI}_j(\mathbf{x}^{(j)*}; R_j) \end{aligned}$$

This inequality shows that mq-EI’s maximum value is greater than the product of expected improvement maxima, which shows that this criterion does not minimize f_1, \dots, f_m jointly. The last term can be further lower bounded, $\prod_{j=1}^m \text{EI}_j(\mathbf{x}^{(j)*}; \mathbf{R}) \geq \prod_{j=1}^m \text{EI}_j(\mathbf{x}^*; \mathbf{R}) = \text{mEI}(\mathbf{x}^*; \mathbf{R})$.

For q-mEI, a trivial lower bound is the mEI maximum: $\max_{\mathbf{x}^{(1)}, \dots, \mathbf{x}^{(q)}} \text{q-mEI}(\{\mathbf{x}^{(1)}, \dots, \mathbf{x}^{(q)}\}; \mathbf{R}) \geq \max_{\mathbf{x}} \text{mEI}(\mathbf{x}; \mathbf{R}) = \text{mEI}(\mathbf{x}^*; \mathbf{R})$.

These lower bounds indicate that more improvement is expected within the q steps than during a single mEI step.

3.4 Experiments: parallel targeting

We now investigate the capabilities of the parallel version of mEI. First, a comparison between q-mEI and mq-EI is made on the basis of two simple one-dimensional quadratic functions. This example illustrates that, as seen from the formulas, q-mEI is the correct multi-point extension of mEI. Then, q-mEI is compared with the sequential mEI. The q-mEI (4) and mq-EI (3) criteria are calculated by Monte Carlo simulation with $N = 10,000$ samples. Because the optimization of the criteria is carried out in a $q \times d$ dimensional space and the gradients are not available, in all experiments, we restrict to $q = 2$ parallel iterates.

3.4.1 Comparison between mq-EI and q-mEI

To compare q-mEI with mq-EI, we consider a simple example with $d = 1$, $q = 2$ and $m = 2$ quadratic objective functions:

$$\min_{x \in [0,1]} (f_1(x), f_2(x))$$

where $f_1(x) = 0.6x^2 - 0.24x + 0.1$ and $f_2(x) = x^2 - 1.8x + 1$, whose minima are respectively 0.2 and 0.9. The multi-objective optimality conditions [29] show that the Pareto set is $\mathcal{P}_X = [0.2, 0.9]$ and the Pareto front $\mathcal{P}_Y = \{\mathbf{y} = (f_1(x), f_2(x))^\top, x \in [0.2, 0.9]\}$. f_1 and f_2 are plotted in Figure 5, both in the design space $X = [0, 1]$ and in the objective space, the Pareto set/front being highlighted.

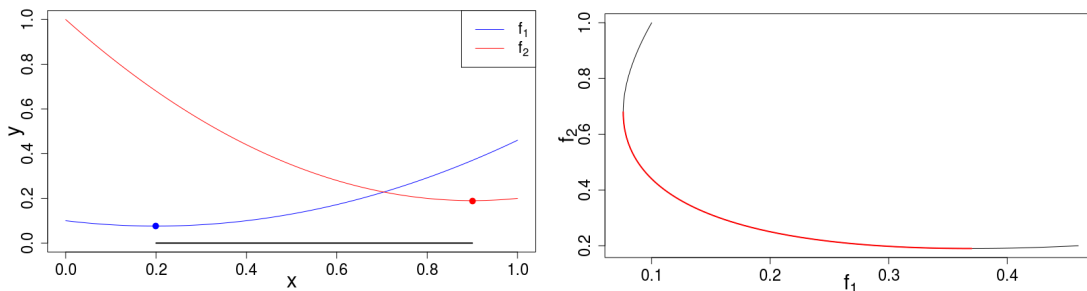


Figure 5: Left: f_1 and f_2 in the design space. The dot corresponds to each minimum, and the black line to \mathcal{P}_X . Right: f_1 and f_2 in the objective space. The red part of the curve is the Pareto front.

Two independent GPs $Y_1(\cdot)$ and $Y_2(\cdot)$ are fitted to $n = 3$ data points. We take $x^{(1)} = 0.05$, $x^{(2)} = 0.6$ and $x^{(3)} = 0.95$. Figure 6 shows the kriging predictors $\hat{f}_1(x)$ and $\hat{f}_2(x)$, as well as the empirical Pareto front.

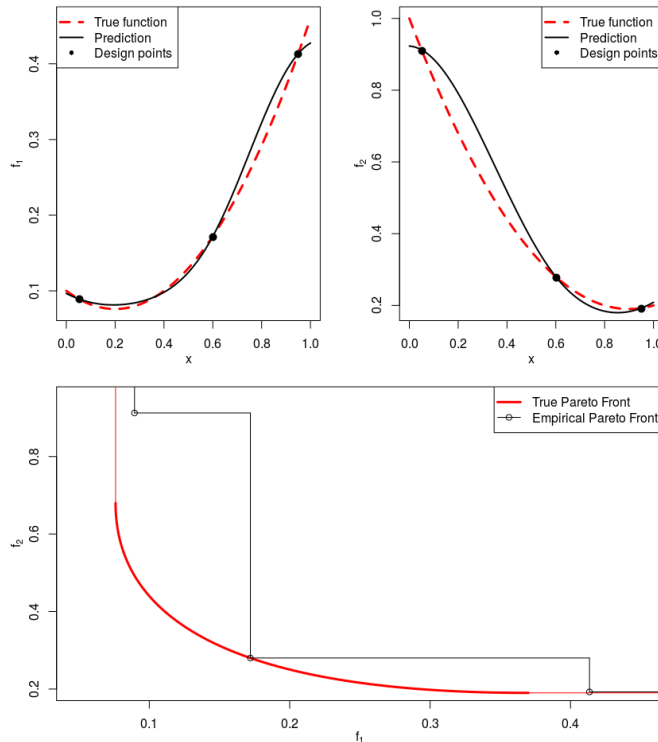


Figure 6: Top: Kriging predictor for f_1 and f_2 . Bottom: empirical Pareto front

Let us take the non-dominated reference point $\mathbf{R} = (0.15, 0.42)^\top$ that we will use both with mq-EI and q-mEI. With that reference point shown in green in Figure 7, domination of \mathbf{R} is achieved when $x \in [0.42, 0.55]$.

In the first experiment, we fix $x^{(n+1)}$ and search the $x^{(n+2)}$ maximizing mq-EI($\{x^{(n+1)}, x^{(n+2)}\}; \mathbf{R}$) and q-mEI($\{x^{(n+1)}, x^{(n+2)}\}; \mathbf{R}$). Two different settings are considered. In the first one, $x^{(n+1)} = 0.2$ which corresponds to an extreme point of the Pareto set that does not dominate \mathbf{R} . In the second case, $x^{(n+1)} = 0.46$ is chosen, a point of the Pareto set whose image dominates \mathbf{R} . Figure 7 illustrates these settings.

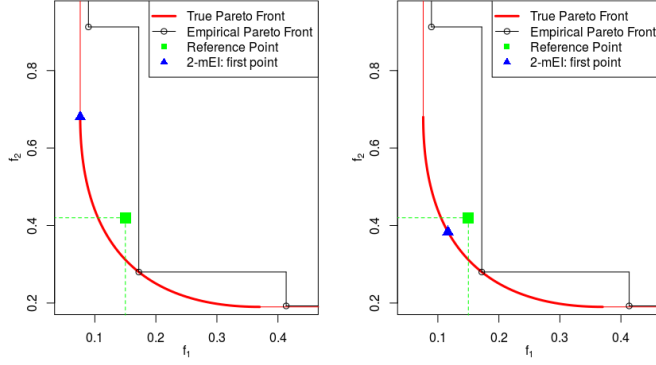


Figure 7: Image of the chosen $x^{(n+1)}$ for the two settings (blue triangle). For each experiment, the goal is to find $x^{(n+2)}$ maximizing $\text{mq-EI}(\{x^{(n+1)}, x^{(n+2)}\}; \mathbf{R})$ or $\text{q-mEI}(\{x^{(n+1)}, x^{(n+2)}\}; \mathbf{R})$.

The results are presented in Figures 8 and 9. In the first setting, $x^{(n+1)} = 0.2$ is a bad choice as its response does not dominate \mathbf{R} . q-mEI gives $x^{(n+2)} = 0.49$ which is the (one-step) mEI maximizer, hence a relevant input given $x^{(n+1)}$ and $\mathbf{f}(x^{(n+2)})$ dominates \mathbf{R} . On the contrary, mq-EI separates the objectives. As $x^{(n+1)}$ is a good input for objective f_1 , the criterion reaches its maximum when $x^{(n+2)} = 0.86$, which is a good input when considering f_2 alone. Figure 6 tells us that 0.86 is almost the minimizer of $\hat{f}_2(x)$. However, the goal was to dominate \mathbf{R} , which is not the case here.

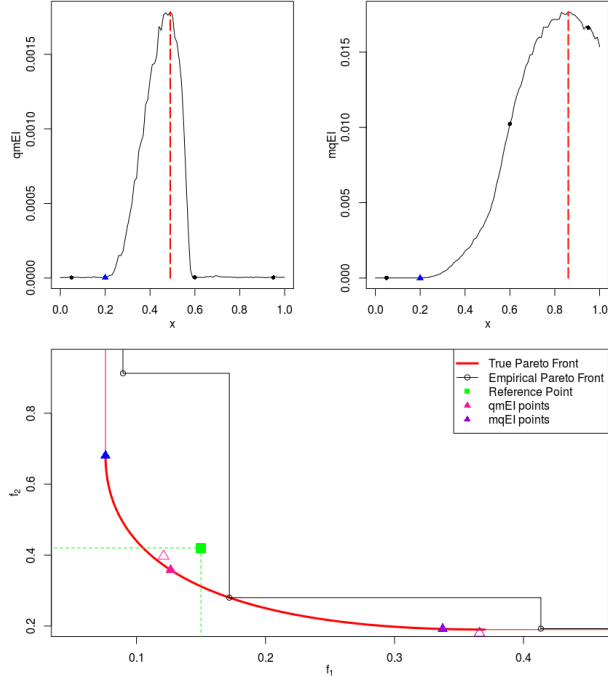


Figure 8: Setting 1: $x^{(n+1)} = 0.2$ (blue triangle). Top: $\text{q-mEI}(\{x^{(n+1)}, x\}; \mathbf{R})$ (left) and $\text{mq-EI}(\{x^{(n+1)}, x\}; \mathbf{R})$ (right) criteria for the second input in the design space. The maximum is achieved at different locations for both criteria. Also notice that for training points $x^{(i)}$ (black dots), $\text{mq-EI}(\{x^{(n+1)}, x^{(i)}\}; \mathbf{R}) \neq \text{mEI}(x^{(n+1)}; \mathbf{R}) \approx 0$, contrarily to $\text{q-mEI}(x^{(n+1)}, x^{(i)})$. Bottom: corresponding values for $\mathbf{f}(x^{(n+2)})$. q-mEI provides an input whose image (pink) dominates \mathbf{R} . On the contrary, m-qEI's solution concentrates on the minimization of the second objective (purple). The transparent triangles correspond to the kriging predictions at $x^{(n+2)}$.

In the second setting, $x^{(n+1)} = 0.46$ is a “good point” as it dominates \mathbf{R} . q-mEI leads to $x^{(n+2)} = 0.53$ whose image also dominates \mathbf{R} . Notice that as 0.46 is chosen for $x^{(n+1)}$, the point that jointly maximizes q-mEI with that first point is slightly larger than 0.48 (the mEI maximizer), and provides more diversity in $\mathcal{I}_{\mathbf{R}}$. The second input for maximizing mq-EI is $x^{(n+2)} = 0.83$, again a good input for minimizing f_2 alone, which is almost the same as in the previous case. Yet again, $\mathbf{f}(x^{(n+2)})$ does not dominate \mathbf{R} .

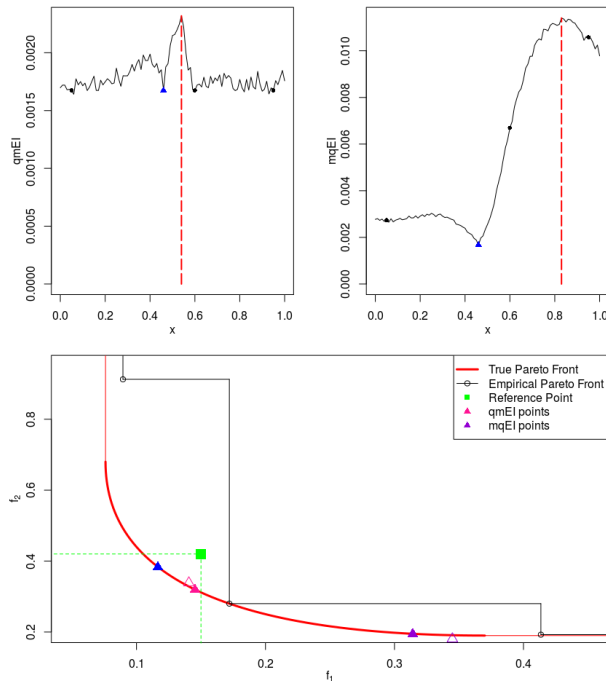


Figure 9: Setting 2: $x^{(n+1)} = 0.46$ (blue triangle). Top: q-mEI($\{x^{(n+1)}, x\}; \mathbf{R}$) (left) and mq-EI($\{x^{(n+1)}, x\}; \mathbf{R}$) (right) criteria for the second input in the design space whose maximum is again achieved at different locations. Bottom: corresponding values for $\mathbf{f}(x^{(n+2)})$. q-mEI provides an input whose image (pink) also dominates \mathbf{R} . On the contrary, mq-EI returns an input which concentrates on the minimization of the second objective (purple). The transparent triangles correspond to the kriging predictions at $x^{(n+2)}$.

Now, we optimize directly mq-EI and q-mEI with respect to both inputs $x^{(n+1)}$ and $x^{(n+2)}$. The optimal batches are $\{0.43, 0.51\}$ for q-mEI and $\{0.26, 0.87\}$ for mq-EI. Figure 10 shows that these inputs lead to $\mathcal{I}_{\mathbf{R}}$ with q-mEI. On the contrary, the images of mq-EI’s optimum are located at the boundaries of the Pareto front. None of them is in $\mathcal{I}_{\mathbf{R}}$ which was our primary goal. Figure 10 further indicates that q-mEI is high when both inputs are in the part of the design space that leads to domination of \mathbf{R} (gray box) contrarily to mq-EI, which is high when each input leads to the domination of one component of \mathbf{R} .

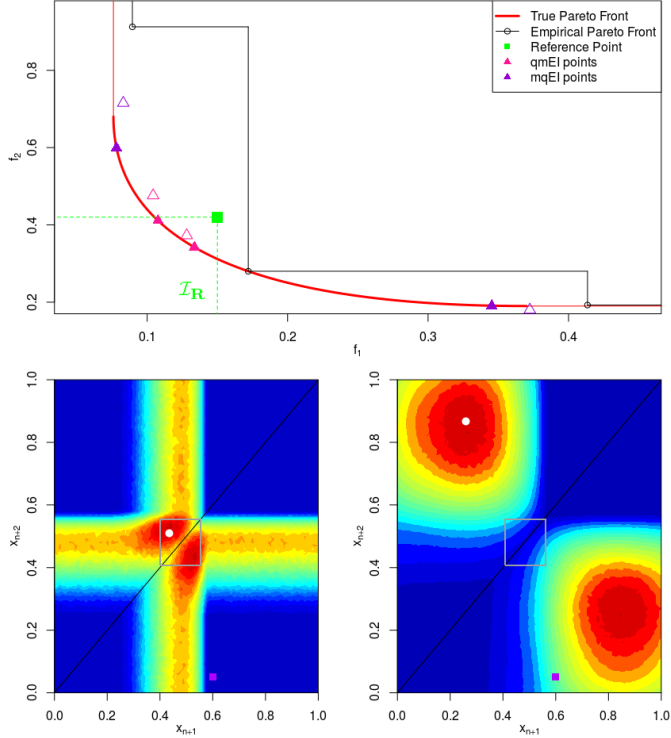


Figure 10: 2 points mq-EI and q-mEI. Top: values obtained in the objective space using both criteria. The images of $x^{(n+1)}$ and $x^{(n+2)}$ returned by q-mEI (pink) both dominate \mathbf{R} . None of those returned by mq-EI (purple) are in $\mathcal{I}_{\mathbf{R}}$, they rather try to improve over each component of \mathbf{R} individually. Transparent triangles correspond to the kriging mean predictor. Bottom: criterion value for $\{x^{(n+1)}, x^{(n+2)}\}$. For q-mEI (left), the best x 's, in dark red, are indeed those which lead to domination of \mathbf{R} (gray box). Conversely, for mq-EI (right), good x 's are designs whose images are *objective-wise* improving upon \mathbf{R} . The white dots correspond to both optima. Notice that for two training points, q-mEI = 0 whereas mq-EI \neq 0, illustrated by the purple square at $(x^{(2)}, x^{(1)})$.

3.4.2 Parallel targeting of the center of the Pareto front

We now compare q-mEI with the sequential mEI. We use the Meta NACA benchmark [17] in $d = 8$ dimensions and with $m = 2$ objectives, as in Section 2.3, for which at each iteration, the center of the Pareto front is estimated and targeted. Figure 11 reports a typical run of q-mEI with 2×10 iterations and a run of mEI after 10 and 20 iterations. The bottleneck of the optimization problem being the computation of $\mathbf{f}(\cdot)$, q-mEI with 2×10 iterations and mEI with 10 iterations roughly need the same time. We also consider this benchmark in $d = 22$ dimensions, where q-mEI with 2×25 iterations is compared with mEI after 25 and 50 iterations.

For numerical comparison, the hypervolume indicator [44] computed in \mathcal{I}_w (defined in [17]), averaged over 10 runs is given in Table 3.4.2. It corresponds to a restriction of the indicator to a narrow central part of the Pareto front. $w = 0.3$ is used to restrict to approximately 30% of

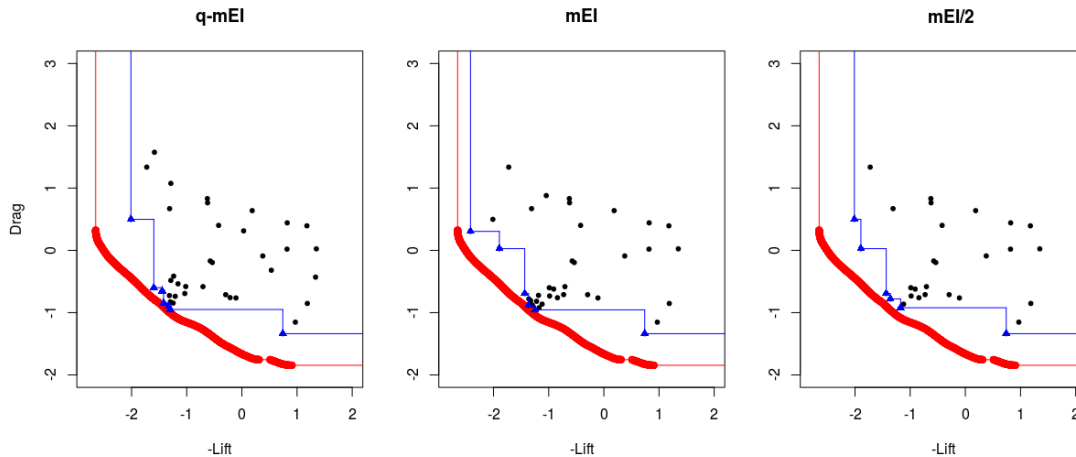


Figure 11: Example of optimization using q-mEI (left) with 2×10 additional designs, and mEI with 20 (center) or 10 (right) iterations. At the same number of calls to $\mathbf{f}(\cdot)$, q-mEI's approximation front (blue) at the center is slightly improved compared to mEI (right). For an equal number of added values, q-mEI and mEI provide equivalent approximations of the center.

the most central solutions of the true Pareto front. The column mEI corresponds to optimizations using the same amount of additional points (i.e. respectively 20 and 50), and the column mEI/2 to those runs after 10 and 25 iterations, the same number of calls to $\mathbf{f}(\cdot)$ than q-mEI, hence with comparable temporal cost.

Criterion	q-mEI	mEI	mEI/2
$d = 8$	0.234 (0.022)	0.265 (0.035)	0.209 (0.067)
$d = 22$	0.327 (0.045)	0.353 (0.048)	0.318 (0.048)

Table 1: Hypervolume indicator computed in $\mathcal{I}_{0.3}$ for q-mEI, mEI and mEI after twice less iterations. At the same temporal cost, q-mEI outperforms mEI.

These empirical results indicate that for the same number of calls to the expensive functions, q-mEI behaves slightly better than mEI. mEI with the same number of additional designs leads to better results, but at twice the temporal cost. Also notice that the standard deviation (in brackets) is slightly improved with q-mEI, meaning a more stable convergence to the center. The same observations are made when considering the distance to the true center.

4 Conclusions and further work

In this paper, we have described an efficient infill criterion called mEI to guide a multi-objective Bayesian algorithm towards non-dominated targets. We have also singled out one such target by introducing the concept of Pareto front center. Numerical experiments have shown that targeting the center of the Pareto front is feasible within restricted budgets for which the approximation of the entire front would not be feasible. A multi-point extension to the mEI criterion has been proposed which opens the way to targeted Bayesian multi-objective optimization carried out in parallel. At the same temporal cost, q times more experiments can be performed to attain the Pareto front. This criterion, called q-mEI, has only been optimized for $q = 2$ parallel iterates and is still computed using Monte-Carlo simulations. These early experiments have confirmed that wall-clock time benefits are achievable with the multi-point infill criterion q-mEI.

In the spirit of [12, 27, 28], it might be possible to derive an analytical expression for q-mEI and its gradient, an important perspective as it would allow to optimize it efficiently.

References

- [1] Anne Auger, Johannes Bader, Dimo Brockhoff, and Eckart Zitzler. Articulating user preferences in many-objective problems by sampling the weighted hypervolume. In *Proceedings of the 11th Annual conference on Genetic and evolutionary computation*, pages 555–562. ACM, 2009.
- [2] Anne Auger, Johannes Bader, Dimo Brockhoff, and Eckart Zitzler. Investigating and exploiting the bias of the weighted hypervolume to articulate user preferences. In *Proceedings of the 11th Annual conference on Genetic and evolutionary computation*, pages 563–570. ACM, 2009.
- [3] Anne Auger, Johannes Bader, Dimo Brockhoff, and Eckart Zitzler. Theory of the hypervolume indicator: optimal μ -distributions and the choice of the reference point. In *Proceedings of the tenth ACM SIGEVO workshop on Foundations of genetic algorithms*, pages 87–102. ACM, 2009.
- [4] Anne Auger, Johannes Bader, Dimo Brockhoff, and Eckart Zitzler. Hypervolume-based multi-objective optimization: Theoretical foundations and practical implications. *Theoretical Computer Science*, 425:75–103, 2012.
- [5] Slim Bechikh, Marouane Kessentini, Lamjed Ben Said, and Khaled Ghédira. Chap. 4: Preference incorporation in evolutionary multiobjective optimization: A survey of the state-of-the-art. *Advances in Computers*, 98:141–207, 2015.
- [6] Mickaël Binois, David Ginsbourger, and Olivier Roustant. Quantifying uncertainty on Pareto fronts with Gaussian process conditional simulations. *European Journal of Operational Research*, 243(2):386–394, 2015.
- [7] Jürgen Branke, Jurgen Branke, Kalyanmoy Deb, Kaisa Miettinen, and Roman Slowiński. *Multiobjective optimization: Interactive and evolutionary approaches*, volume 5252. Springer Science & Business Media, 2008.

- [8] Jürgen Branke, Kalyanmoy Deb, Henning Dierolf, and Matthias Osswald. Finding knees in multi-objective optimization. In *International conference on parallel problem solving from nature*, pages 722–731. Springer, 2004.
- [9] Dimo Brockhoff, Johannes Bader, Lothar Thiele, and Eckart Zitzler. Directed multiobjective optimization based on the weighted hypervolume indicator. *Journal of Multi-Criteria Decision Analysis*, 20(5-6):291–317, 2013.
- [10] Dimo Brockhoff, Johannes Bader, Lothar Thiele, and Eckart Zitzler. Directed multiobjective optimization based on the weighted hypervolume indicator. *Journal of Multi-Criteria Decision Analysis*, 20(5-6):291–317, 2013.
- [11] John Buchanan and Lorraine Gardiner. A comparison of two reference point methods in multiple objective mathematical programming. *European Journal of Operational Research*, 149(1):17–34, 2003.
- [12] Clément Chevalier and David Ginsbourger. Fast computation of the multi-points expected improvement with applications in batch selection. In *International Conference on Learning and Intelligent Optimization*, pages 59–69. Springer, 2013.
- [13] Michael Emmerich, André Deutz, and Jan Willem Klinkenberg. Hypervolume-based expected improvement: Monotonicity properties and exact computation. In *Evolutionary Computation (CEC), 2011 IEEE Congress on*, pages 2147–2154. IEEE, 2011.
- [14] Paul Feliot. *Une approche Bayésienne pour l’optimisation multi-objectif sous contraintes*. PhD thesis, Université Paris-Saclay, 2017.
- [15] Peter I Frazier and Scott C Clark. Parallel global optimization using an improved multi-points expected improvement criterion. In *INFORMS Optimization Society Conference, Miami FL*, volume 26, 2012.
- [16] Tomas Gal, Theodor Stewart, and Thomas Hanne. *Multicriteria decision making: advances in MCDM models, algorithms, theory, and applications*, volume 21. Springer Science & Business Media, 1999.
- [17] David Gaudrie, Rodolphe Le Riche, Victor Picheny, Benoit Enaux, and Vincent Herbert. Budgeted multi-objective optimization with a focus on the central part of the pareto front-extended version. *arXiv preprint arXiv:1809.10482*, 2018.
- [18] David Ginsbourger, Janis Janusevskis, and Rodolphe Le Riche. Dealing with asynchronicity in parallel gaussian process based global optimization. In *4th International Conference of the ERCIM WG on computing & statistics (ERCIM’11)*, 2011.
- [19] David Ginsbourger and Rodolphe Le Riche. Towards gp-based optimization with finite time horizon. 2009.
- [20] David Ginsbourger, Rodolphe Le Riche, and Laurent Carraro. Kriging is well-suited to parallelize optimization. In *Computational Intelligence in Expensive Optimization Problems*, pages 131–162. Springer, 2010.

- [21] Hisao Ishibuchi, Yasuhiro Hitotsuyanagi, Noritaka Tsukamoto, and Yusuke Nojima. Many-objective test problems to visually examine the behavior of multiobjective evolution in a decision space. In *International Conference on Parallel Problem Solving from Nature*, pages 91–100. Springer, 2010.
- [22] Janis Janusevskis, Rodolphe Le Riche, and David Ginsbourger. Parallel expected improvements for global optimization: summary, bounds and speed-up. 2011.
- [23] Janis Janusevskis, Rodolphe Le Riche, David Ginsbourger, and Ramunas Girdziusas. Expected improvements for the asynchronous parallel global optimization of expensive functions: Potentials and challenges. In *Learning and Intelligent Optimization*, pages 413–418. Springer, 2012.
- [24] Donald R Jones, Matthias Schonlau, and William Welch. Efficient Global Optimization of expensive black-box functions. *Journal of Global optimization*, 13(4):455–492, 1998.
- [25] Andy J Keane. Statistical improvement criteria for use in multiobjective design optimization. *AIAA journal*, 44(4):879–891, 2006.
- [26] Joshua Knowles. ParEGO: A hybrid algorithm with on-line landscape approximation for expensive multiobjective optimization problems. *IEEE Transactions on Evolutionary Computation*, 10(1):50–66, 2006.
- [27] Sébastien Marmin, Clément Chevalier, and David Ginsbourger. Differentiating the multi-point expected improvement for optimal batch design. In *International Workshop on Machine Learning, Optimization and Big Data*, pages 37–48. Springer, 2015.
- [28] Sébastien Marmin, Clément Chevalier, and David Ginsbourger. Efficient batch-sequential bayesian optimization with moments of truncated gaussian vectors. *arXiv preprint arXiv:1609.02700*, 2016.
- [29] Kaisa Miettinen. *Nonlinear multiobjective optimization*, volume 12. Springer Science & Business Media, 1998.
- [30] Ilya Molchanov. *Theory of random sets*, volume 19. Springer, 2005.
- [31] Victor Picheny. Multiobjective optimization using Gaussian process emulators via stepwise uncertainty reduction. *Statistics and Computing*, 25(6):1265–1280, 2015.
- [32] Wolfgang Ponweiser, Tobias Wagner, Dirk Biermann, and Markus Vincze. Multiobjective optimization on a limited budget of evaluations using model-assisted S-metric selection. In *International Conf. on Parallel Problem Solving from Nature*, pages 784–794. Springer, 2008.
- [33] Melina Ribaud. *Krigeage pour la conception de turbomachines: grande dimension et optimisation robuste*. PhD thesis, Université de Lyon, 2018.
- [34] Yoshikazu Sawaragi, Hirotaka Nakayama, and Tetsuzo Tanino. *Theory of multiobjective optimization*, volume 176. Elsevier, 1985.
- [35] Matthias Schonlau. Computer experiments and global optimization. 1997.

- [36] Joshua Svenson. *Computer experiments: Multiobjective optimization and sensitivity analysis*. PhD thesis, The Ohio State University, 2011.
- [37] Joshua Svenson and Thomas J Santner. Multiobjective optimization of expensive black-box functions via expected maximin improvement. *The Ohio State University, Columbus, Ohio*, 32, 2010.
- [38] Evangelos Triantaphyllou. Multi-criteria decision making methods. In *Multi-criteria decision making methods: A comparative study*, pages 5–21. Springer, 2000.
- [39] Andrzej Wierzbicki. The use of reference objectives in multiobjective optimization. In *Multiple criteria decision making theory and application*, pages 468–486. Springer, 1980.
- [40] Andrzej Wierzbicki. Reference point approaches. published in multicriteria decision making: Advances in MCDM models, algorithms, theory, and applications. t. gal, tj stewart and t. hanne, 1999.
- [41] Kaifeng Yang, Andre Deutz, Zhiwei Yang, Thomas Back, and Michael Emmerich. Truncated expected hypervolume improvement: Exact computation and application. In *Evolutionary Computation (CEC), 2016 IEEE Congress on*, pages 4350–4357. IEEE, 2016.
- [42] Kaifeng Yang, Longmei Li, André Deutz, Thomas Back, and Michael Emmerich. Preference-based multiobjective optimization using truncated expected hypervolume improvement. In *Natural Computation, Fuzzy Systems and Knowledge Discovery (ICNC-FSKD), 2016 12th International Conference on*, pages 276–281. IEEE, 2016.
- [43] Milan Zeleny. The theory of the displaced ideal. In *Multiple criteria decision making Kyoto 1975*, pages 153–206. Springer, 1976.
- [44] Eckart Zitzler. *Evolutionary algorithms for multiobjective optimization: Methods and applications*. 1999.